

Blue quantum emitter in hexagonal boron nitride and carbon chain tetramer: proposition of identification

Marek Maciaszek^{1,2,*} and Lukas Razinkovas^{2,3}

¹*Faculty of Physics, Warsaw University of Technology, Koszykowa 75, 00-662 Warsaw, Poland*

²*Center for Physical Sciences and Technology (FTMC), Vilnius LT-10257, Lithuania*

³*Department of Physics/Centre for Materials Science and Nanotechnology, University of Oslo, P.O. Box 1048, Blindern, Oslo N-0316, Norway*

Single photon emitters in hexagonal boron nitride offer a gateway to the future of quantum technologies, yet their identification remains challenging and subject to ongoing debate. We demonstrate through *ab initio* calculations that the optical properties of a carbon chain tetramer are in excellent agreement with the characteristics of a blue quantum emitter in hexagonal boron nitride emitting at 435 nm. Its calculated zero-phonon line energy (2.77 eV) and radiative lifetime (1.6 ns) perfectly align with experimental observations. The relatively weak electron–phonon coupling (Huang–Rhys factor of 1.5) indicates intense emission at the zero-phonon line. Despite the absence of an inversion center in the carbon tetramer, we demonstrate that it exhibits a negligible linear Stark effect, consistent with experimental findings. Additionally, our hypothesis explains the experimental observation that the formation of blue emitters is only possible in samples containing numerous ultraviolet emitters, which are likely identical to carbon dimers.

I. INTRODUCTION

Hexagonal boron nitride (h-BN) has long been employed in nanotechnology, yet recent years have seen a notable surge in attention toward this material, spurred by the discovery of numerous single-photon emitters within h-BN [1]. Its wide bandgap enables it to accommodate single-photon emitters from the near-infrared to ultraviolet spectrum. Notably, many emitters demonstrate high brightness and stability even at room temperature, positioning them as promising candidates for applications in emerging quantum technologies [2–4].

A blue quantum emitter with a zero-phonon line (ZPL) of 2.85 eV (435 nm) in hexagonal boron nitride was observed in 2019 by Shevitski et al. [5]. Subsequently, its optical properties have been extensively explored in numerous studies [5–9]. Its excited state lifetime was determined as 1.8–2.1 ns [8, 9]. The quantum efficiency of the blue emitters was estimated to be at least 20%, making them bright while exhibiting excellent photostability. It was concluded that the defect, being the blue quantum emitter, has no metastable state, and the suggested electronic structure comprises two levels within the bandgap: one fully occupied in the lower half and an empty one in the upper half [6]. Moreover, it was demonstrated that the emitter exhibits a very weak Stark effect induced by out-of-plane fields and a much stronger but almost purely quadratic for in-plane fields [7].

Blue emitters can be created at chosen locations by electron irradiation treatment [8], and this procedure is

efficient only in samples exhibiting a high concentration of ultraviolet (featuring a ZPL of 4.1 eV) emitters [9]. These blue emitters remain stable under annealing treatments up to 800°C [10]. Nonetheless, annealing at 1000°C leads to the disappearance of the blue emitters and the emergence of other emitting centers. The ZPLs of these new emitters are observed across a spectral range from 420 to 480 nm (2.58 to 2.95 eV).

A minimal linear Stark effect has prompted the hypothesis of nitrogen or carbon interstitial defects being responsible for blue emission [7]. This idea was further elaborated with the theory that the negatively charged nitrogen split interstitial defect is the source of the blue emission [11]. Although the calculated properties of the nitrogen interstitial largely align with experimental data, there are two significant issues with this assignment: (1) the computed radiative lifetime is 54 ns, and (2) the observed correlation between blue and UV emitters, typically attributed to carbon dimers, cannot be simply explained.

In the following, we demonstrate that all these experimental observations can be well explained by the properties of the carbon chain tetramer $(C_B C_N)_2$, where four carbon atoms substitute on four neighbouring sites within the h-BN lattice (see Fig. 1). Our reasoning is based on four arguments: (1) the simultaneous presence of both blue and UV emitters becomes understandable when identifying the 435 nm emitter as a carbon-based complex, (2) the ZPL of the carbon tetramer, calculated to be 2.77 eV, closely matches the experimental value, (3) the computed radiative lifetime of 1.6 ns shows excellent agreement with experimental findings, and (4) the linear Stark effect is predicted to be negligible.

The carbon chain tetramer can exist in two geometric configurations: *cis* or *trans* (see Fig. 1). While calculated

* marek.maciaszek@pw.edu.pl

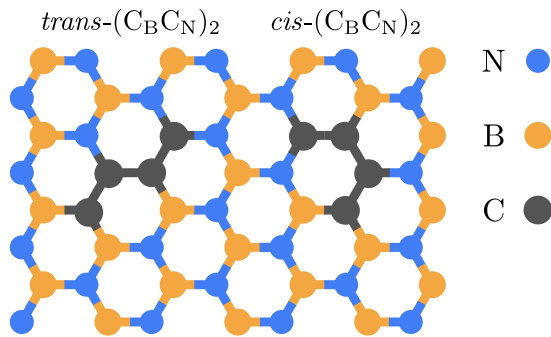


FIG. 1. Cis and *trans* configurations of carbon tetramers $(C_B C_N)_2$ in h-BN.

results favor the *trans* conformer, which exhibits better agreement with experimental findings, both conformers will be analyzed and discussed.

II. METHODOLOGY

Ab initio calculations were performed using spin-polarized density functional theory (DFT) as implemented in VASP code [12]. The projector augmented wave (PAW) method was employed with a plane wave energy cutoff set to 500 eV [13]. In calculations, we used a 288-atom hexagonal supercell (equivalent to a $6 \times 6 \times 2$ arrangement of the primitive cell), sampling the Brillouin zone at the Γ point only. Ionic relaxation was conducted until forces fell below 0.01 eV/Å.

The formation energies of the defect (refer to Sec. III A) were calculated using the Heyd–Scuseria–Ernzerhof (HSE) hybrid density functional [14]. To accurately capture the material’s band gap, the mixing parameter α was adjusted from the default value of 0.25 to 0.31, achieving a band gap of 5.95 eV. This computational setup yielded lattice constants $a = 2.490$ Å and $c = 6.558$ Å, which show good agreement with experimental measurements ($a = 2.506$ Å and $c = 6.603$ Å [15]). Furthermore, the formation enthalpy of the compound was calculated to be -2.89 eV, aligning well with the experimental value of -2.60 eV [16].

The formation energy E_f of a carbon chain tetramer is expressed as [17, 18]

$$E_f(q) = E_D(q) - E_H - 4\mu_C + 2(\mu_B + \mu_N) + q(E_V + E_F) + E_{\text{corr}}$$

where E_D and E_H represent the total energies of the supercell with and without a tetramer, respectively. Additionally, μ_B , μ_N , and μ_C denote the chemical potentials of boron, nitrogen, and carbon, respectively. When calculating the formation energy, we assumed the chemical potential of carbon to be equal to that in bulk graphite. This represents the maximum possible value of μ_C , indicating the highest carbon availability during growth. It is worth noting that $\mu_B + \mu_N = \mu_{\text{BN}} = E_H/n$, where n

represents the number of formula units in the supercell ($n = 144$ in our case). Therefore, E_f does not depend on the individual chemical potentials of B or N. q is the charge state of the tetramer, E_V stands for the energy of the valence band maximum (VBM), and E_{corr} is a correction that describes the interaction between charged defects in periodic supercells. E_{corr} value was calculated using the Freysoldt–Neugebauer–Van de Walle methodology [19]. E_F is the Fermi level with respect to E_V . The charge-state transition level $\varepsilon(q/q')$ is defined as the value of E_F for which the formation energies of two charge states, q and q' , are equal.

In modeling electronic properties (Sec. III B), we utilized the meta-GGA $r^2\text{SCAN}$ exchange–correlation functional [20, 21], which provided a band gap of 4.83 eV. The optimized lattice constants, $a = 2.502$ Å and $c = 6.515$ Å, along with the formation enthalpy of -2.89 eV (equal to the HSE result), exhibit good alignment with experimental findings, demonstrating the effectiveness of $r^2\text{SCAN}$ in simulating bulk properties despite underestimation of the band gap.

Our decision to utilize the $r^2\text{SCAN}$ functional stemmed from the HSE functional’s tendency to overestimate ZPL energies. While $r^2\text{SCAN}$ tends to slightly underestimate ZPL energies, its performance in the context of diamond defects, for instance, yields mean absolute errors for ZPL similar to those obtained using HSE with a standard mixing parameter ($\alpha = 0.25$) [22]. Elevating α to match the experimental band gap implies a potential widening of HSE’s deviation in ZPL energy predictions. Furthermore, such adjustment of α raises concerns regarding the accuracy of calculations, as this approach may not satisfy Koopman’s theorem [11]. However, for a comprehensive evaluation, all calculations were also performed using HSE with $\alpha = 0.31$, and the comparison of results obtained with both methodologies is provided in the Supplementary Material.

Van der Waals interactions were taken into account by employing the Grimme-D3 method in HSE calculations [23] and the nonlocal rVV10 method [24–27] in $r^2\text{SCAN}$ calculations.

III. RESULTS AND DISCUSSION

A. Formation and temperature stability

The formation energy of the neutral carbon chain tetramer (*trans* conformer) is 3.30 eV (Fig. 2). Its neutral charge state is stable in a wide range of the Fermi level: charge-state transition levels are 1.24 and 5.16 eV above the VBM for $(+/0)$ and $(0/-)$, respectively. The $2+$ and $2-$ charge states were found not to be stable.

Regarding the *cis* conformer, its formation energy is lower by 0.06 eV than that of the *trans* conformer, and its charge-state transition levels are $\varepsilon(+/0) = 1.07$ eV and $\varepsilon(0/-) = 5.23$ eV above the VBM. Since further analysis of the formation and temperature stability focuses on

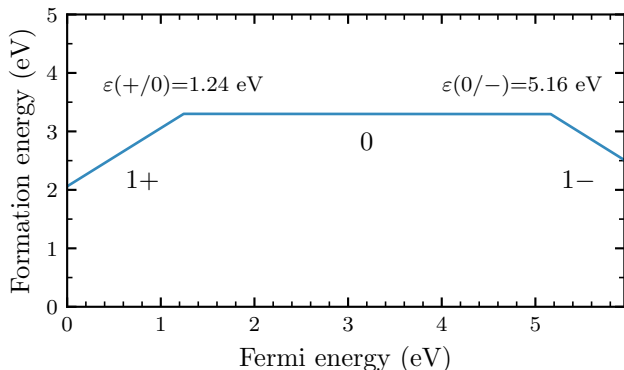


FIG. 2. Formation energy of $trans\text{-}(C_B C_N)_2$ as a function of the Fermi level.

the neutral charge state, where the formation energies are nearly identical for both conformers, the conclusions are applicable to the *cis* conformer as well. Quantitative results pertain to the *trans* conformer.

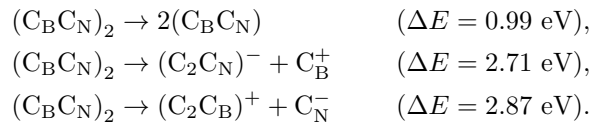
Although the formation energy of carbon tetramers is not particularly high, blue emitters are not formed under equilibrium conditions but through electron irradiation treatment, and the number of fabricated emitters depends on the electron dose [8, 9]. It was demonstrated that the formation of blue emitters is most efficient in samples exhibiting a high concentration of 4.1 eV emitters [9]. Since the 4.1 eV emitters are commonly identified with carbon dimers $C_B C_N$ [28], this experimental observation suggests that blue emitters are carbon related defects. Furthermore, it was speculated that blue emitters are formed through the restructuring of carbon dimers induced by the electron beam, which breaks the bonds and enhances the drift of ionized atoms [9]. This aligns well with our hypothesis, as a carbon tetramer can be formed from two dimers. Alternatively, one could posit that carbon tetramers are not formed by merging two dimers but rather by the fragmentation of larger carbon clusters induced by the electron beam. The presence of such clusters should correlate with the large concentration of carbon dimers, as both phenomena are caused by high carbon density in the h-BN sample.

The blue emitters remain stable up to 800°C. However, after annealing at 1000°C for 1 hour, it was demonstrated that the blue emitters disappear, and other emitters emerge, exhibiting various ZPLs, mostly distributed between 2.58 and 2.95 eV [10]. In the following, we discuss the results of this experiment in the context of the tetramer model.

Experimental observations suggest that annealing at 1000°C sufficiently enhances diffusion to restore thermodynamic equilibrium within the timeframe of the experiment. The existence of tetramers under thermodynamic equilibrium at 1000°C is unlikely due to their high for-

mation energy. Even assuming the maximal value of the carbon chemical potential, the density of tetramers at 1000°C is $3 \times 10^{10} \text{ cm}^{-3}$. Assuming a flake thickness of 50 nm, this density implies one tetramer per square with a side length of 25 μm , exceeding the area examined in [10]. We propose that the disappearance of blue emitters is caused by the dissociation of tetramers, which can be conceptualized as spontaneous fragmentation induced by high temperature. The presence of smaller carbon defects is more likely due to their lower formation energies.

When one of the bonds in a tetramer breaks, smaller carbon complexes such as dimers, trimers, or monomers are formed. The following are three possible scenarios of the dissociation of a tetramer:



Here, ΔE describes the energetic cost of such a reaction, calculated as the difference in formation energies between substrates and products. These values were estimated using theoretical data provided in [29]. According to the ΔE values, the most probable scenario appears to be the dissociation into two dimers. However, the ΔE values for the latter two reactions correspond to two isolated products (i.e., a monomer and a trimer at a large distance). In actual reactions, the monomer and trimer are in close proximity to each other just after dissociation. Consequently, strong electrostatic attraction reduces ΔE , and this reduction can be estimated to be as significant as 1 eV, or even slightly higher, for certain configurations. Thus, the formation of monomers and trimers is also likely to occur.

The observed diversity in ZPLs can also be attributed to differences in distances between charged carbon defects, such as monomers and trimers, resulting in variations in electrostatic interactions. ZPLs of C_B^+ and C_N^- pairs exhibit a strong dependence on the distance between carbon atoms, as demonstrated in [30]. The similar phenomenon of the emergence of other emitters after annealing was also noted for carbon-based visible (red) emitters, and the optical properties of the produced emitter families are similar in both cases [10]. This observation aligns well with our identification.

The annealing temperature allows for the estimation of the activation energy of the rate-limiting process. Assuming a typical phonon frequency in h-BN of 10^{14} s^{-1} [31] and a process rate on the order of 1 s^{-1} , we can approximate its value to be between 3.0 and 3.5 eV. This value is similar to the migration barrier of boron vacancies in h-BN, which is 3.09 eV for V_B^- [32]. It can be expected that electron irradiation creates vacancies at a high density. If these vacancies are present close to the tetramer, they can mediate carbon diffusion. However, due to their high formation energies, boron vacancies eventually vanish. It can be hypothesized that since

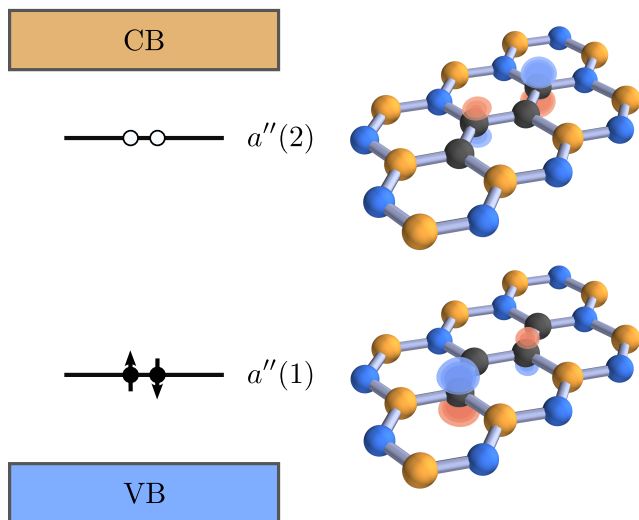


FIG. 3. Kohn–Sham electronic energy level diagram and corresponding orbital isosurfaces for the *trans* conformer.

boron vacancies are produced in the vicinity of irradiated spots and thus close to blue emitters, they are able to mediate carbon diffusion; however, after some time, they are annealed.

B. Electronic structure and optical properties

In the analysis that follows, we focus on the neutral charge state of the tetramer, whose electronic structure features two distinct levels within the bandgap: a lower-lying, fully occupied level, and an upper-lying, vacant level, as shown in Fig. 3. The electronic structure of the blue emitter proposed in [6], deduced from the photostability of the emission, closely resembles the structure of the tetramer presented here.

Our computations demonstrate that both conformers of the carbon chain tetramer present C_s symmetry. The localized states within the band gap belong to the irreducible representation a'' , with the lower-energy state denoted as $a''(1)$ and the higher-energy state as $a''(2)$ (see Fig. 3). This configuration indicates that all bound electronic states of neutral charge state exhibit A' symmetry, implying that both permanent (diagonal) and transition (off-diagonal) dipole moments align within the two-dimensional plane of the h-BN lattice.

In the molecular orbital picture, the ground state is a closed-shell singlet represented by wavefunction $|S_0\rangle = |a''(1)\bar{a}''(1)\rangle$, where the notation without and with a bar distinguishes spin-up from spin-down molecular orbitals. The transition to singly excited singlet $|S_1\rangle$ and triplet $|T\rangle$ states involves excitation from $a''(1)$ to $a''(2)$. For $m_s = 1$ projection, the triplet state is depicted by a single determinant wavefunction $|T\rangle = |a''(1)a''(2)\rangle$. The excited singlet state, $|S_1\rangle$, on the other hand, emerges as a strongly-correlated, multi-determinant state: $|S_1\rangle =$

$1/\sqrt{2}(|a''(1)\bar{a}''(2)\rangle - |a''(2)\bar{a}''(1)\rangle)$. Due to its multi-determinant nature, traditional DFT cannot directly model $|S_1\rangle$. Thus, we determine its energy using an approximate spin-purification approach [33, 34]. It involves two distinct energy computations: one for the single-determinant triplet state and another for a mixed spin determinant, $|M\rangle = |a''(1)\bar{a}''(2)\rangle$. The energy of the excited singlet state is approximately given by [28]:

$$E(S_1) = 2E(M) - E(T). \quad (1)$$

We employed the delta-self-consistent-field (Δ SCF) methodology, constraining occupations of Kohn–Sham orbitals, for computing single-determinant energy terms $E(M)$ and $E(T)$. Concerning the geometric structure, given that the excited singlet and triplet states possess identical orbital configurations and differ only due to exchange splitting, it indicates that the geometry of the excited state S_1 is close to that of the triplet state. Therefore, we approximated the geometry of S_1 by the relaxed geometry of the T state.

The ZPL energies have been calculated as 2.77 eV for the *trans* conformer and 3.10 eV for the *cis* conformer. Since the r^2 SCAN method tends to slightly underestimate ZPL energies, the calculated value for the *trans* conformer closely matches the experimental result of 2.85 eV. Notably, using the relaxed geometry of the mixed spin state (M state) to represent the singlet excited state S_1 leads to ZPL energies lower by about 0.04 eV (all results are detailed in the Supplemental Material). This observation is consistent with the above assumption that the geometry of the triplet state closely approximates that of the excited singlet state.

Electronic relaxation from the singlet excited state S_1 can proceed through two pathways: a radiative transition to the singlet ground state or intersystem crossing to the triplet state T , located 0.35 eV below S_1 . Given the relatively large exchange splitting of 0.35 eV between the singlet and triplet states, coupled with minor differences in potential energy surfaces (leading to small Huang–Rhys factor), it is expected that the non-radiative lifetime substantially exceeds the radiative lifetime, thereby making radiative decay the predominant mechanism.

The radiative lifetime, τ_{rad} , can be estimated using equation:

$$\frac{1}{\tau_{\text{rad}}} = \frac{n_r E_{\text{ZPL}}^3 \mu^2}{3\pi \epsilon_0 \hbar^4 c^3}, \quad (2)$$

where n_r is the refractive index of h-BN, E_{ZPL} is the ZPL energy, μ is the optical transition dipole moment, and ϵ_0 is the vacuum permittivity. The transition dipole moment, μ , is estimated utilizing the expressions derived for molecular orbital states:

$$\mu = \langle S_0 | \sum_i \mathbf{r}_i | S_1 \rangle = \sqrt{2} \langle a''(1) | \mathbf{r} | a''(2) \rangle, \quad (3)$$

where the final single-particle expression is obtained by applying the Condon rules for determinantal states. We

then calculate $\langle a''(1)|\mathbf{r}|a''(2)\rangle$ using single-particle Kohn–Sham orbitals determined from the triplet electronic and geometric configuration, a common practice in DFT calculations.

With the ZPL energy set to an experimental value of 2.85 eV and using $n_r = 2.25$ [35, 36], the radiative lifetime for the *trans* conformer is calculated to be 1.6 ns. This finding aligns closely with experimental lifetimes reported between 1.8 and 2.1 ns [8, 9]. The calculated transition dipole moment is 1.77 eÅ. For the *cis* conformer, τ_{rad} is 2.5 ns, with a transition dipole moment of 1.42 eÅ.

To quantify the electron-phonon coupling strength, we calculated the Huang–Rhys factor S within the effective mode approximation, following the methodology outlined in Ref. [37]. The Huang–Rhys factor, S , characterizes the mean number of phonons emitted during electronic transitions. The energy released due to lattice relaxation after transitioning to the ground state was calculated to be 0.20 eV. We determined the effective phonon frequency to be $\hbar\omega = 134$ meV, resulting in a Huang–Rhys factor of $S = 1.50$. This factor is pivotal for estimating of the luminescence intensity fraction within the zero-phonon line (ZPL), referred to as the Debye–Waller factor (DWF). Employing the single-mode approximation allows for an estimation of $\text{DWF} \approx e^{-S}$, an approximation applicable in the limit $\hbar\omega/E_{\text{ZPL}} \ll 1$. This yields a theoretical Debye–Waller factor of $\text{DWF} = 0.22$. Using a more rigorous formula, as explained in the Supplementary Material, results in a marginally increased value of 0.28. The experimental measurements of the DWF, which were reported as 0.26 in Ref. [5] and 0.40 in Ref. [8], place our calculated value in agreement with the experimental findings. Regarding the *cis* conformer, the calculated values are $S = 1.91$ and $\hbar\omega = 122$ meV.

HSE results confirm the general conclusions drawn from $r^2\text{SCAN}$ calculations. HSE with $\alpha = 0.31$ yields higher values of the ZPL, 3.29 eV and 3.58 eV for the *trans* and *cis* conformers, respectively. Since HSE typically overestimates ZPL, especially with an assumed α larger than its standard value of 0.25, HSE values can be considered upper limits for the ZPL. Consequently, $r^2\text{SCAN}$ provides lower limits. The experimental value of 2.85 eV falls within this estimated range for the *trans* conformer. Concerning the radiative lifetime, its values are slightly smaller when calculated using HSE (1.4 ns and 2.2 ns for *trans* and *cis*, respectively). All results obtained with both functionals are presented in the Supplementary Material. Additionally, all data are calculated for both approximations of the geometry of the singlet excited state: by the geometry of the triplet (T) and the mixed spin (M) states.

Finally, we examine results related to the Stark effect. Experiments revealed that an out-of-plane electric field causes a negligible linear Stark shift, estimated at 0.04 meV/V nm⁻¹, and no quadratic dependency was detected in this direction. Conversely, a significant quadratic shift in the ZPL was noted under in-plane electric fields, with the linear component remaining very

small [7].

It is often assumed that the absence of a linear Stark effect implies the defect has a center of inversion symmetry. However, this assertion should be correctly understood in reverse: the presence of an inversion symmetry center in a defect guarantees the absence of a linear Stark effect. Nevertheless, there are instances where a defect lacking inversion symmetry does not exhibit a linear Stark effect or demonstrates a very faint one. For instance, this phenomenon may occur when the electric field induces identical shifts in both optically active energy levels [38].

As previously mentioned, theory predicts no linear Stark shift for an out-of-plane field according to group theory. The experimentally observed minimal linear Stark shift in the out-of-plane direction could be attributed to sample inhomogeneity.

For the in-plane electric field, we introduce a straightforward *ab initio* methodology to evaluate the linear Stark shift. Within the first-order perturbation theory, the ZPL shift is given by:

$$\Delta E_{\text{ZPL}} = -\mathbf{E}e \left(\langle S_1 | \sum_i \mathbf{r}_i | S_1 \rangle - \langle S_0 | \sum_i \mathbf{r}_i | S_0 \rangle \right), \quad (4)$$

where \mathbf{E} denotes the applied electric field. Leveraging molecular orbital wavefunctions, this shift can be expressed using single-particle matrix elements:

$$\Delta E_{\text{ZPL}} = -\mathbf{E}e (\langle a''(2) | \mathbf{r} | a''(2) \rangle - \langle a''(1) | \mathbf{r} | a''(1) \rangle), \quad (5)$$

which can be calculated from Kohn–Sham single-particle states. The amplitudes of the permanent dipole moments are calculated to be smaller than 10⁻³ eÅ for both $a''(1)$ and $a''(2)$. Insignificant values of amplitudes can also be inferred from the symmetry of the spatial distribution of the charge density (see Fig. 3). The obtained results demonstrate that the linear Stark shift for the *trans* tetramer under in-plane electric fields should be negligibly small, which is consistent with experimental observations. A similar understanding can be applied to the *cis* conformer, for which the vanishing of the linear Stark shift is also expected.

IV. CONCLUSIONS

In summary, we presented the results of *ab initio* modeling of the carbon chain tetramer in hexagonal boron nitride. Its calculated optical properties match very well with experimental characteristics of the blue emitter. The calculated ZPL of 2.77 eV closely aligns with the experimental value of 2.85 eV, and the radiative lifetime of 1.6 ns is in good agreement with the measured values of 1.8–2.1 ns. Moreover, we demonstrated that the electron-phonon coupling is relatively weak ($S = 1.5$), and the calculated Debye–Waller factor is 0.28, in good accordance with the experimental results (0.26 and 0.40). The linear Stark effect should be absent or extremely

weak for both in-plane and out-of-plane external fields, consistent with experimental observations.

Additionally, we discussed experimental studies of the formation and annealing of blue emitters, proposing that the carbon chain tetramer provides a coherent explanation for their observations. Specifically, our identification of the blue emitter as the carbon tetramer elucidates why the fabrication of blue emitters is efficient only in h-BN samples containing numerous UV emitters. Furthermore, the postulated dissociation of the tetramer with temperature provides an explanation for the observed formation of other emitters with similar ZPLs after annealing at 1000°C, attributing it to the emergence of carbon

monomers, dimers and trimers at different distances.

ACKNOWLEDGMENTS

Research was funded by the Warsaw University of Technology within the Excellence Initiative: Research University (IDUB) programme. Computational resources were provided by the Interdisciplinary Center for Mathematical and Computational Modelling (ICM), University of Warsaw (Grant No. GB81-6), and the High Performance Computing center “HPC Saulėtekis” in the Faculty of Physics, Vilnius University.

-
- [1] Caldwell J D, Aharonovich I, Cassabois G, Edgar J H, Gil B and Basov D N 2019 *Nature Reviews Materials* **4** 552–567 ISSN 2058-8437 URL <https://doi.org/10.1038/s41578-019-0124-1>
- [2] Tran T T, Bray K, Ford M J, Toth M and Aharonovich I 2016 *Nature Nanotechnology* **11** 37–41 ISSN 1748-3395 URL <https://doi.org/10.1038/nnano.2015.242>
- [3] Sajid A, Ford M J and Reimers J R 2020 *Reports on Progress in Physics* **83** 044501 URL <https://dx.doi.org/10.1088/1361-6633/ab6310>
- [4] Aharonovich I, Tettienne J P and Toth M 2022 *Nano Letters* **22** 9227–9235 pMID: 36413674 (Preprint <https://doi.org/10.1021/acs.nanolett.2c03743>) URL <https://doi.org/10.1021/acs.nanolett.2c03743>
- [5] Shevitski B, Gilbert S M, Chen C T, Kastl C, Barnard E S, Wong E, Ogletree D F, Watanabe K, Taniguchi T, Zettl A and Aloni S 2019 *Phys. Rev. B* **100**(15) 155419 URL <https://link.aps.org/doi/10.1103/PhysRevB.100.155419>
- [6] Zhigulin I, Yamamura K, Ivády V, Gale A, Horder J, Lobo C J, Kianinia M, Toth M and Aharonovich I 2023 *Materials for Quantum Technology* **3** 015002 URL <https://dx.doi.org/10.1088/2633-4356/acb87f>
- [7] Zhigulin I, Horder J, Ivády V, White S J, Gale A, Li C, Lobo C J, Toth M, Aharonovich I and Kianinia M 2023 *Phys. Rev. Appl.* **19**(4) 044011 URL <https://link.aps.org/doi/10.1103/PhysRevApplied.19.044011>
- [8] Fournier C, Plaud A, Roux S, Pierret A, Rosticher M, Watanabe K, Taniguchi T, Buil S, Quélin X, Barjon J, Hermier J P and Delteil A 2021 *Nature Communications* **12** 3779 ISSN 2041-1723 URL <https://doi.org/10.1038/s41467-021-24019-6>
- [9] Gale A, Li C, Chen Y, Watanabe K, Taniguchi T, Aharonovich I and Toth M 2022 *ACS Photonics* **9** 2170–2177 (Preprint <https://doi.org/10.1021/acsphotonics.2c00631>) URL <https://doi.org/10.1021/acsphotonics.2c00631>
- [10] Chen Y, Gale A, Yamamura K, Horder J, Condos A, Watanabe K, Taniguchi T, Toth M and Aharonovich I 2023 *Applied Physics Letters* **123** 041902 ISSN 0003-6951 (Preprint https://pubs.aip.org/aip/apl/article-pdf/doi/10.1063/5.0155311/18056302/041902_1.5.0155311.pdf) URL <https://doi.org/10.1063/5.0155311>
- [11] Ganyecz Á, Babar R, Benedek Z, Aharonovich I, Barcza G and Ivády V 2024 *Nanoscale* **16**(8) 4125–4139 URL <http://dx.doi.org/10.1039/D3NR05811E>
- [12] Kresse G and Furthmüller J 1996 *Phys. Rev. B* **54**(16) 11169–11186 URL <https://link.aps.org/doi/10.1103/PhysRevB.54.11169>
- [13] Blöchl P E 1994 *Phys. Rev. B* **50**(24) 17953–17979 URL <https://link.aps.org/doi/10.1103/PhysRevB.50.17953>
- [14] Heyd J, Scuseria G E and Ernzerhof M 2003 *The Journal of Chemical Physics* **118** 8207–8215 ISSN 0021-9606 (Preprint https://pubs.aip.org/aip/jcp/article-pdf/118/18/8207/19093575/8207_1_online.pdf) URL <https://doi.org/10.1063/1.1564060>
- [15] Paszkowicz W, Pelka J B, Knapp M, Szyszko T and Podsiadlo S 2002 *Applied Physics A* **75** 431–435 ISSN 1432-0630 URL <https://doi.org/10.1007/s003390100999>
- [16] Tomaszkiwicz I 2002 *Pol. J. Chem.* **76** 891–899
- [17] Zhang S B and Northrup J E 1991 *Phys. Rev. Lett.* **67**(17) 2339–2342 URL <https://link.aps.org/doi/10.1103/PhysRevLett.67.2339>
- [18] Freysoldt C, Grabowski B, Hickel T, Neugebauer J, Kresse G, Janotti A and Van de Walle C G 2014 *Rev. Mod. Phys.* **86**(1) 253–305 URL <https://link.aps.org/doi/10.1103/RevModPhys.86.253>
- [19] Freysoldt C, Neugebauer J and Van de Walle C G 2009 *Phys. Rev. Lett.* **102**(1) 016402 URL <https://link.aps.org/doi/10.1103/PhysRevLett.102.016402>
- [20] Sun J, Ruzsinszky A and Perdew J P 2015 *Phys. Rev. Lett.* **115**(3) 036402 URL <https://link.aps.org/doi/10.1103/PhysRevLett.115.036402>
- [21] Furness J W, Kaplan A D, Ning J, Perdew J P and Sun J 2020 *The Journal of Physical Chemistry Letters* **11** 8208–8215 pMID: 32876454 (Preprint <https://doi.org/10.1021/acs.jpcllett.0c02405>) URL <https://doi.org/10.1021/acs.jpcllett.0c02405>
- [22] Maciaszek M, Žalandauskas V, Silkinis R, Alkauskas A and Razinkovas L 2023 *The Journal of Chemical Physics* **159** 084708 (Preprint https://pubs.aip.org/aip/jcp/article-pdf/doi/10.1063/5.0154319/18102318/084708_1.5.0154319.pdf) URL <https://doi.org/10.1063/5.0154319>
- [23] Grimme S 2006 *Journal of Computational Chemistry* **27** 1787–1799 (Preprint <https://onlinelibrary.wiley.com/doi/pdf/10.1002/jcc.20495>) URL <https://onlinelibrary.wiley.com/doi/abs/10.1002/jcc.20495>

- [24] Dion M, Rydberg H, Schröder E, Langreth D C and Lundqvist B I 2004 *Phys. Rev. Lett.* **92**(24) 246401 URL <https://link.aps.org/doi/10.1103/PhysRevLett.92.246401>
- [25] Román-Pérez G and Soler J M 2009 *Phys. Rev. Lett.* **103**(9) 096102 URL <https://link.aps.org/doi/10.1103/PhysRevLett.103.096102>
- [26] Klimeš J c v, Bowler D R and Michaelides A 2011 *Phys. Rev. B* **83**(19) 195131 URL <https://link.aps.org/doi/10.1103/PhysRevB.83.195131>
- [27] Peng H, Yang Z H, Perdew J P and Sun J 2016 *Phys. Rev. X* **6**(4) 041005 URL <https://link.aps.org/doi/10.1103/PhysRevX.6.041005>
- [28] Mackoīt-Sinkevičienė M, Maciaszek M, Van de Walle C G and Alkauskas A 2019 *Applied Physics Letters* **115** 212101 ISSN 0003-6951 (Preprint https://pubs.aip.org/aip/apl/article-pdf/doi/10.1063/1.5124153/13286483/212101_1.online.pdf) URL <https://doi.org/10.1063/1.5124153>
- [29] Maciaszek M, Razinkovas L and Alkauskas A 2022 *Phys. Rev. Mater.* **6**(1) 014005 URL <https://link.aps.org/doi/10.1103/PhysRevMaterials.6.014005>
- [30] Auburger P and Gali A 2021 *Phys. Rev. B* **104**(7) 075410 URL <https://link.aps.org/doi/10.1103/PhysRevB.104.075410>
- [31] Geick R, Perry C H and Rupprecht G 1966 *Phys. Rev.* **146**(2) 543–547 URL <https://link.aps.org/doi/10.1103/PhysRev.146.543>
- [32] Weston L, Wickramaratne D, Mackoīt M, Alkauskas A and Van de Walle C G 2018 *Phys. Rev. B* **97**(21) 214104 URL <https://link.aps.org/doi/10.1103/PhysRevB.97.214104>
- [33] Ziegler T, Rauk A and Baerends E J 1977 *Theoretica chimica acta* **43** 261–271
- [34] von Barth U 1979 *Phys. Rev. A* **20**(4) 1693–1703 URL <https://link.aps.org/doi/10.1103/PhysRevA.20.1693>
- [35] Lee S Y, Jeong T Y, Jung S and Yee K J 2019 *physica status solidi (b)* **256** 1800417 (Preprint <https://onlinelibrary.wiley.com/doi/pdf/10.1002/pssb.201800417>) URL <https://onlinelibrary.wiley.com/doi/abs/10.1002/pssb.201800417>
- [36] Grudin D V, Ermolaev G A, Baranov D G, Toksumakov A N, Voronin K V, Slavich A S, Vyshnevyy A A, Mazitov A B, Kruglov I A, Ghazaryan D A, Arsenin A V, Novoselov K S and Volkov V S 2023 *Mater. Horiz.* **10**(7) 2427–2435 URL <http://dx.doi.org/10.1039/D3MH00215B>
- [37] Alkauskas A, Lyons J L, Steiauf D and Van de Walle C G 2012 *Phys. Rev. Lett.* **109**(26) 267401 URL <https://link.aps.org/doi/10.1103/PhysRevLett.109.267401>
- [38] Udvarhelyi P, Nagy R, Kaiser F, Lee S Y, Wrachtrup J and Gali A 2019 *Phys. Rev. Appl.* **11**(4) 044022 URL <https://link.aps.org/doi/10.1103/PhysRevApplied.11.044022>